Tailoring Shear-Stiff, Mica-like Nanoplatelets

Michael W. Möller,[†] Ulrich A. Handge,[‡] Daniel A. Kunz,[†] Thomas Lunkenbein,[†] Volker Altstädt,[‡] and Josef Breu[†,*]

[†]Lehrstuhl für Anorganische Chemie I and [‡]Lehrstuhl für Polymere Werkstoffe, Universität Bayreuth, Universitätsstrasse 30, 95447 Bayreuth, Germany

Exploitation of the marked anisotropic bonding inherent to layered compounds like clays,[1] layered double hydroxides,[2−4] layered chalcogenides,[5−9] phosphates,[10] and zeolite precursors[11] paves the way for an "anisotropic top down" approach by exfoliation.[12,13] The reduction of the thickness h of lamellar crystallites by cleavage eventually produces nanoplatelets with a dramatically increased portion of surface/interface atoms and with very high aspect ratios.

Such two-dimensional nanomaterials have recently been used in various new fields of nanotechnology; for instance, responsive Bragg-stacks,[14] superb diffusion barriers,[15] artificial nacre,[16−19] and reinforcing fillers in hybrid materials like polymer layered silicate nanocomposites (PLSNs).[20−24] In particular for the latter two applications, the aspect ratio and/or mechanical properties are of key importance.

Among the plethora of layered compounds known, swelling 2:1 layered silicates stand out due to their rich interlamellar reactivity, which, in principle, allows a facile tuning of the strength of the interactions between consecutive layers in the stack. This pronounced interlamellar reactivity can mainly be attributed to the reactivity of interlayer cations. Moreover, hydration/solvation of interlayer cations (swelling) or cation exchange with bulky onium compounds (organophilization) concomitantly increases the basal spacing and thus decreases the cohesion between lamellae in the stack. Larger basal spacings reduce the attractive Coulomb forces between the positively charged interlamellar space and the negatively charged silicate lamellae significantly by $F \sim 1/d^2$. This reduces the shear strength of the clay stacks, which in turn promotes the efficiency of exfoliation at a given shear rate.

On one hand, low shear strength is advantageous for maximizing the aspect ratio. On the other hand, it is detrimental for reinforcement because the interactions along the stacking direction are noncovalent in nature, and therefore, the interlamellar space bears a lower load as compared to the silicate lamellae, which may lead to failure at the interlayer.[25] The shear stiffness is, in turn, related to the flexural rigidity of the reinforcing nanoplatelet, which increases with $\sim h^3$ and the strength of the interaction along the stacking direction.[26] Consequently, there will be an optimum combination of aspect ratio and height of the reinforcing platelet.
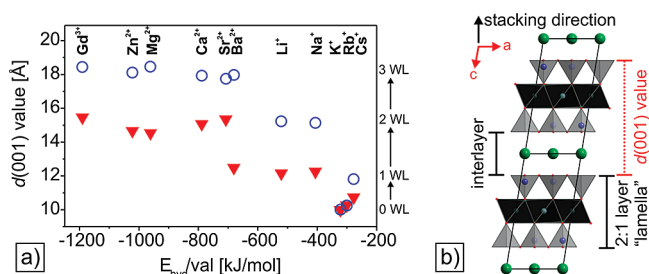
In summary, an ideal material would allow for switching between shear-labile and shear-stiff states of reinforcing nanoplatelets. The first state will be utilized to optimize the height for any given lateral dimension of the platelets, while the latter will help to minimize failure by gliding along the interlamellar space.

ABSTRACT This work introduces a novel facile method to produce shear-stiff, mica-like nanoplatelets by efficient exfoliation. The essence of this procedure is the nonreversible alteration of the interlamellar reactivity of a synthetic fluorohectorite by simple cation exchange. The possibility of switching from highly hydrated to collapsed interlayers permits a highly efficient exfoliation in the swollen state while providing shear-stiffness in the collapsed state. This method restricts cation exchange in the mica-like nanoplatelets to the outer surfaces, which represents a significant advantage for use in nanocomposites as compared to conventional organoclays which contain up to 40%/wt of organocations. It is expected that this new type of rigid, shear-stiff, clay-based nanoplatelets will be superior for reinforcement when used in composite materials like polymer layered silicate nanocomposites or artificial nacre.

KEYWORDS: nanoplatelet · exfoliation · shear-stiff · mica-like · PLSN · layered silicates

Figure 1. Hydration states of fluorohectorite obtained from PXRD-measurements as a function of selected interlayer cations. The d(001) values for moist (○) and air-dried (▼; 40% RH) samples are plotted *versus* the enthalpy of hydration *per* valence of the interlayer cations (a). Structural scheme of fluorohectorite (b). A stack of two unit cells is displayed with the viewing direction along the *b*-axis.

The degree of swelling of 2:1 layered silicates is determined by the interplay of the hydration enthalpy of interlayer cations and the Coulomb attraction between silicate lamellae and interlayers, which scales with the charge density of the lamellae and hence the degree of isomorphous substitution. Since the layer charge can be easily controlled for synthetic (fluoro-)hectorites, the Coulomb attraction may thereby be tuned to a level where the degree of hydration varies drastically for different interlayer cations.

In the following, we present a synthetic fluorohectorite that permits switching between a highly hydrated, shear-labile Mg^{2+} form and a completely nonhydrated, nonswelling, mica-like, shear-stiff K^+ form of the same fluorohectorite. An additional benefit of the latter nonswelling state is the possibility of distinguishing between internal (=interlayer space) and external (=external basal planes and edges) particle surfaces, which minimizes the amount of compatibilizer necessary to adjust the adhesion between the filler and matrix when using these materials as reinforcing fillers in composite materials.

RESULTS AND DISCUSSION

Hydration Properties of Synthetic Fluorohectorites and Their Effect on the Efficiency of Exfoliation. Smectites like montmorillonites of natural origin suffer from inherent deficiencies like small particle sizes and pronounced heterogeneities of charge distribution, which, in turn, lead to nonuniform interlamellar reactivity.[27] For instance, at any given relative humidity, different interlayers will accept different hydration states corresponding to heterogeneities of charge density.[28] Melt synthesis, however, produces clays with superb charge homogeneity, and consequently a uniform interlamellar reactivity.[29,30] Additionally, synthesis gives full control over composition, and thus over layer charge and physical properties like electric conductivity.[31−33] In this way, clay materials can be designed with different applications in mind. For instance, materials become available with huge lateral dimensions comparable to micas, but with interlamellar reactivities typical of smectites.

The clay used here is a synthetic fluorohectorite, $\{Na_{0.5}\}^{inter}[Mg_{2.5}Li_{0.5}]^{oct}\langle Si_4\rangle^{tet}O_{10}F_2$ (Na-Hec), with a layer charge *per* formula unit (*p.f.u.*) of 0.5. Due to the high homogeneity of charge density of this Na-Hec, the transitions between different well-defined hydration states are observed as discrete steps (Figure 1a, Scheme 1, and
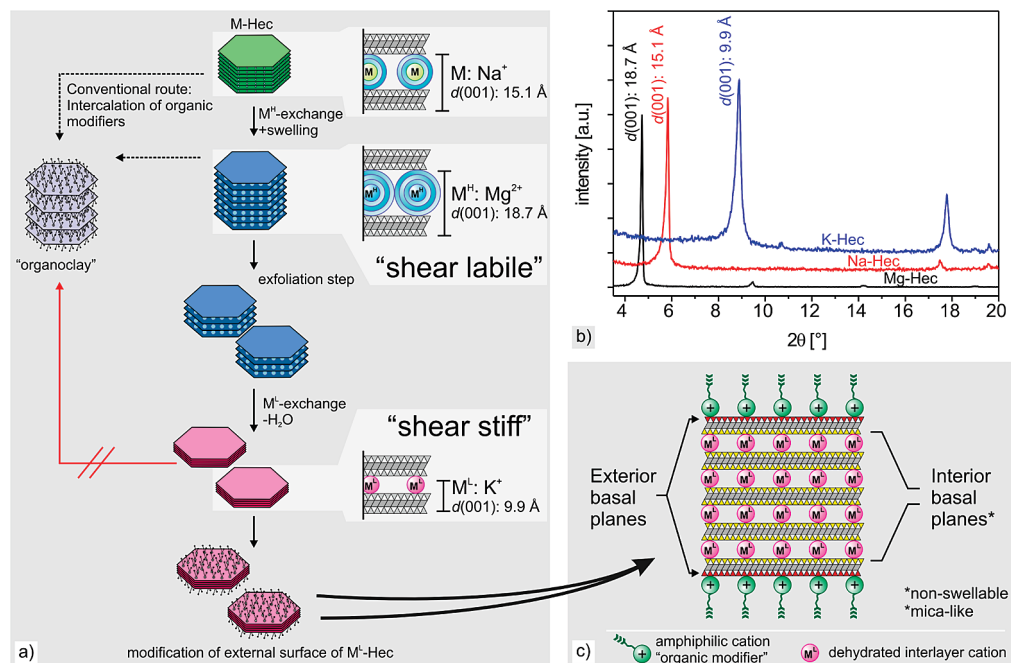
Scheme 1. Production of shear-stiff, mica-like nanoplatelets and the selective modification of their external basal planes: (a) M, M^H, and M^L indicate interlayer cations with $|E_{hyd}|$: $M^L < M < M^H$. The PXRD pattern (b) illustrates three different stages of hydration exemplified with K-Hec, Na-Hec, and Mg-Hec (moist samples). A schematic cross-section of a surface-modified tactoid with nonswellable interlayers is given in panel c. Internal and external basal planes are marked in yellow and red, respectively.
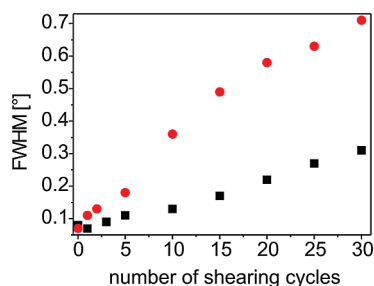
Figure 2. Evolution of FWHM values of the (001)-reflections for Na-Hec (■; 2WL) and Mg-Hec (●; 3WL) with the number of shearing cycles applied.

Supporting Information, Figure S1). Additionally, the stage of hydration depends strongly on the type of interlayer cation, and to a lesser extent, on the layer charge.[34−37] All samples were prepared by ion exchange from pristine Na-Hec. Figure 1a gives an overview of the degree of hydration of the same hectorite with respect to varying interlayer cations. A structural scheme of fluorohectorite is illustrated in Figure 1b. Transitions between different hydration states appeared at an E_{hyd} per valence of approximately −700 kJ/mol and between −322 and −406 kJ/mol. Interestingly, the Cs-Hec showed anomalous behavior in water. Despite a very low E_{hyd} of −277 kJ/mol, Cs-Hec forms a 1WL-hydrate (WL: water layer). This interlamellar reactivity is attributed to the large radius of the Cs^+ ion, which results in significantly increased basal spacing of the non-swollen state as compared to K-Hec or Rb-Hec.[33] Thus, the relative stability of the dehydrated reference state is diminished, fostering hydration.

Na-Hec forms the two-water layer hydrate (2WL) with an interlayer distance $d(001)$ of 15.1 Å when immersed in water. The exchange of Mg^{2+} for Na^+, which has a higher enthalpy of hydration (−1922 and −406 kJ mol^{-1} respectively), increases the $d(001)$ value to 18.7 Å, representing the 3WL-hydrate. In contrast to both hydrated cations, the exchange with K^+ (E_{hyd}: −322 kJ mol^{-1}) yields a collapsed and nonswelling mica-like material (0WL) with $d(001) = 9.9$ Å, even when immersed in water.

These well-defined stages of swelling enable the interlamellar reactivity to be tuned, allowing for switching between shear-labile and shear-stiff lamellar stacks. Increasing the $d(001)$ value of the layered silicate in aqueous dispersion (moist samples) by intercalating cations with high E_{hyd} promotes more efficient cleavage along the swollen interlamellar spaces. The attractive Coulomb force between the polyanionic silicate lamellae and the interlayer cations thereby decreases by approximately d^2. Additionally, interlayer water represents an efficient lubricant. Figure 2 compares the FWHM (full width at half-maximum) values of the (001)-reflections as obtained by powder X-ray-diffraction (PXRD) of Na-Hec and Mg-Hec exposed to the same number of shearing cycles in a microfluidizer. According to Scherrer,[38] the FWHM values of the (001)-

reflections can be related to the stack height. Thinner stacks have larger corresponding FWHM values. Although FWHM values are dominantly influenced by the size of the coherently scattering domains, for example, the tactoid height in case of the (00*l*)-reflections, some other factors like strain, random interstratification or textural effects may additionally influence the peak broadening. Hence we prefer to compare the neat FWHM values instead of calculating the absolute stack heights.

Even after 30 shearing cycles in a microfluidizer, a rational (00*l*)-series is observed (Supporting Information, Figure S3). Thus, a spontaneous delamination into singular lamellae as observed for laponite-type Li-hectorites can be ruled out.[39] As indicated by the steady increase of the FWHM values with the number of shearing cycles applied, the stacks are efficiently exfoliated. The evolution of the particle size distribution with the number of shearing cycles (Supporting Information, Figure S2) indicates that the stacks are indeed preferentially exfoliated by shearing, but are much less frequently broken. To a first approximation, the hydrodynamic radii recorded in the static light scattering experiment correlate well with the lateral dimensions of the nanoplatelets.[40] The hydrodynamic radii decrease strongly during the initial cycles, which can be attributed mainly to the dispersion of aggregates produced in the melt synthesis. After completion of this initial desegregation (from cycle 10 onward), the median of the particle size distribution enters a plateau which only changes slowly with additional shearing cycles, while the FWHM values continue to increase steadily (Figure 2). From the combination of FWHM values and particle size distributions, it may be concluded that thinner stacks with increased aspect ratio are produced upon shearing. Figure 2 clearly demonstrates the strong influence of the hydration state and thus the basal spacing on the efficiency of the exfoliation. Both plots of the FWHM after shearing increase considerably, but the slope of Mg-Hec (3WL) shows an almost 3-fold increase as compared to the Na-Hec (2WL). Note that, to a first approximation, the FWHM values correlate well with the number of shearing cycles. This suggests that the average thickness and thus the aspect ratio of the nanoplatelets can be tuned by the number of shearing cycles. Moreover, exfoliating a highly hydrated state (M^H-Hec) is not only more efficient as compared to less hydrated forms, it will also help to minimize the undesired fracture of clay platelets. Smaller numbers of shearing cycles are required to achieve the desired height of nanoplatelets, corresponding to a certain number of layer stacks respectively, to ensure maximum aspect ratios.

Subsequent to exfoliation and optimization of the aspect ratio, metamorphosis of the shear-labile nanoplatelets into a nonhydrated, shear-stiff, mica-like form (M^L-Hec) was easily accomplished by replacing Mg^{2+}
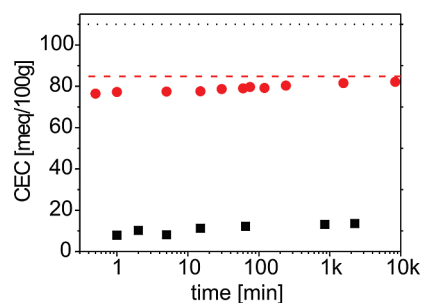
Figure 3. Adsorption kinetics of K-Hec (■) and K-MMT (●) as determined by the adsorption of aqueous [Cu(trien)]$^{2+}$ at room temp. The results are expressed as cation exchange capacities (CEC). Dotted and dashed lines represent the CEC determined for the corresponding Na-Hec (···) and Na-MMT (---), respectively.

with interlayer cations with a low enthalpy of hydration such as K^{+}. After collapse of the interlamellar space by dehydration, the interlayers are no longer accessible under standard conditions (room temp and exchange times shorter than 1 day). This stepwise metamorphosis cannot be observed for natural montmorillonite (MMT) because of the lower layer charge and the inhomogeneity of the charge density. The total cation exchange capacity (CEC) of the synthetic Na-Hec and a typical natural Na-MMT is 110 meq 100 g^{-1} and 86 meq 100 g^{-1}, respectively. Without any shearing, both clays were transformed into the K^{+}-form by ion-exchange. After drying at 120 °C, the kinetics of the cation exchange were investigated by measuring the evolution of the adsorption of [Cu(trien)]$^{2+}$ (trien = triethylene tetramine) over time (Figure 3). As expected for a strongly adsorbing and highly selective cation like [Cu(trien)]$^{2+}$, for K-MMT an amount corresponding to the total CEC was adsorbed instantly. Contrarily, the amount of [Cu(trien)]$^{2+}$ adsorbed onto K-Hec after one minute is only approximately 7% of the total CEC. This low residual CEC is attributed to external basal planes of the stacks that are still accessible, whereas the collapsed interlayers do not contribute to the CEC of the K-Hec. The amount of [Cu(trien)]$^{2+}$ adsorbed increases only slightly with prolonged exchange times underlining the observation that collapsed, K^{+}-exchanged interlayers no longer show significant interlamellar reactivity.

Limitation of the cation exchange to external basal planes is corroborated by measuring the evolution of CEC and BET-surface areas with the number of shearing cycles applied. For this, Mg-Hec was exposed to increasing numbers of shearing cycles in a Microfluidizer in order to achieve different degrees of exfoliation. Exfoliation transforms interlamellar spaces into outer surfaces of increasingly thinner nanoplatelets. The surface/volume ratio will thus increase nonlinearly with progressing exfoliation. Figure 4 demonstrates the expected change of the specific surface area of platelets with respect to their height and diameter. Calculations for uniform hexagonal platelets show the massive influ-
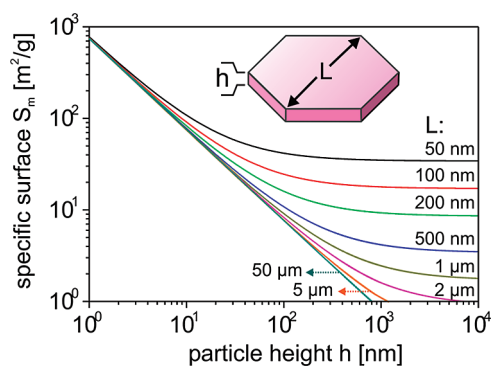

Figure 4. Calculation of the total specific surface area of uniform hexagonal platelets, with diameters L ranging from 50 nm to 50 μm with respect to the particle height h. The density of the particles is assumed to be 2.7 g/cm^3, the density of unhydrated hectorite.

ence of exfoliation on the amount of specific surface area S_m (note the double logarithmic scale). Theoretical values for 1-nm thick hexagonal platelets—what comes close to the height of single clay lamellae—range from 741 to 775 m^2/g for particles with diameters from 50 μm to 50 nm (please see Supporting Information for details of the calculation).

The exfoliated nanoplatelets were then transformed into collapsed K-Hec, and CEC, FWHM values, and BET-surface areas were determined (Figures 5a,b). The increase of FWHM values, which correspond to the stack heights, correlate well with the CEC observed for the outer basal surfaces, and the BET surface areas enlarge concomitantly. Again, the pristine sample (0 shearing
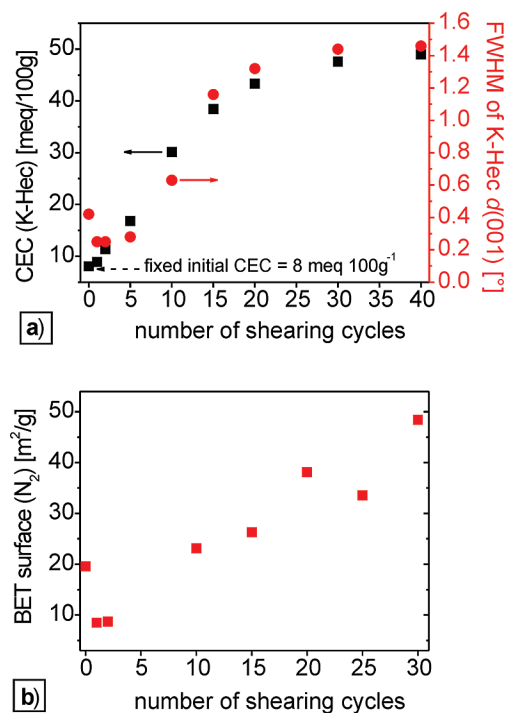
Figure 5. Cation exchange capacities (CEC) and FWHM values (a) and the corresponding BET surface areas (b) for a series of K-Hec with varying degrees of exfoliation as prepared by shearing Mg-Hec. The CEC was determined after a 10-min exchange with [Cu(trien)]$^{2+}$.
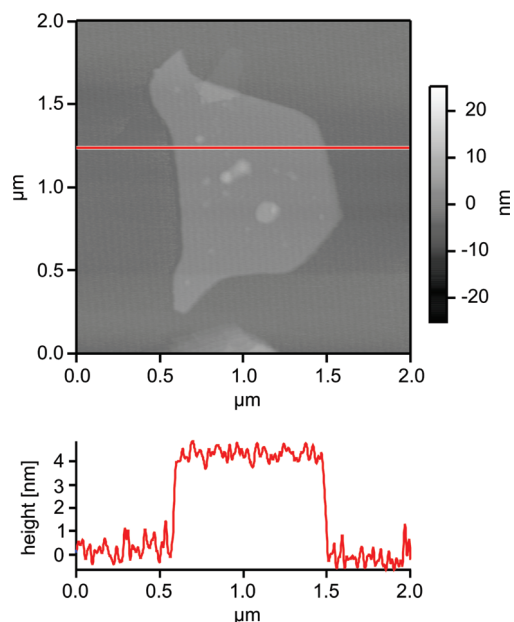
Figure 6. AFM image of a K-Hec nanoplatelet prepared by cation exchange with KCl from exfoliated Mg-Hec (10 shearing cycles). The red line is a cross-sectional height profile.

cycles) shows anomalous behavior, which in line with the particle size changes discussed above, may be explained by aggregates that are destroyed in the initial cycles.

All data underscore the ability to adjust the average height of nanoplatelets by controlling the number of shearing cycles. The reduction of the thickness h by exfoliation eventually produces nanoplatelets with a dramatically increased portion of surface/interface atoms and very large aspect ratios. Figure 6 shows an AFM image of a typical nanoplatelet of K-Hec, as obtained after 10 shearing cycles. The height of *ca.* 4 nm indicates 4 silicate lamellae in the stack (d(001) = 0.99 nm), while the aspect ratios of the irregularly shaped nanoplatelets range between 250 and 375. The CEC of the outer basal surfaces of this nanoplatelet would be 25% of the total CEC. This value correlates well with the average value (27.5 meq 100 g^{-1}) found for K-Hec after 10 shearing cycles (Figure 5a).

Advantages of Novel Nanoplatelets for Reinforcing Applications. The most obvious applications for these manufactured mica-like nanoplatelets would be as reinforcing fillers in PLSN or in artificial nacre. For both of these applications, the aspect ratio, the mechanical properties of the inorganic reinforcing nanoplatelets, and the quality of surface modification to ensure compatibility of filler and matrix are the key issues that will determine the degree of improvement of properties by compounding. Generally, a larger aspect ratio of the nanofillers leads to a more pronounced reinforcement of the polymer matrix, an effect that has been theoretically described by the Halpin−Tsai equations.[41] For example, the exfoliation of layered silicates in polyamide 6

increases the tensile modulus and resistance against crack propagation.[42]

Evidently, for such anisometric and anisotropic fillers, the preferred orientation of the reinforcing platelets in the composite and the directionality of their mechanical properties has to be considered. Obviously, a comprehensive discussion of all possible combinations is beyond the scope of this paper. The following discussion will focus on flexural rigidity and shear modulus.

Clay-based fillers have a long history, but the Toyota process was the most important development making the class of organically modified layered silicates (organoclays) a part of modern material science.[43,44] Meanwhile, many commercial suppliers offer organically modified clays based on natural smectites (such as Cloisite and Nanomer) to improve various physical properties of plastic materials.[45] All commercial organoclays are prepared *via* complete cation exchange in which all interlayer and surface cations are replaced by organic cations (Scheme 1). Loading the clay with bulky cationic organic modifiers increases the basal spacing d(001) and makes the polar surfaces organophilic.[46] In the Toyota process, the nanocomposite is then formed by *in situ* polymerization. The interlayer cations act as initiators and polymerize the co-intercalated monomers. As the polymer chain grows in the interlamellar space, adjacent lamellae are pushed apart and the stacks are fully delaminated into 1-nm thick singular lamellae. However, industry prefers to manufacture PLSNs by melt compounding. Generally, the goal is to achieve delamination during compounding by further expansion of the interlayer space of the organoclays by partial intercalation of polymer chains.

However, careful examination of TEM sections of PLSN produced by melt compounding shows that delamination is hardly ever complete, and stacks of lamellae are present instead.[25] From a mechanical point of view, these intercalated stacks need to be treated as sandwich type reinforcing nanoplatelets, which consist of a "soft" interlamellar region and a "stiff" silicate lamella. Brune and Bicerano emphasized that the incomplete delamination of clay stacks has a tremendous detrimental effect on the reinforcement efficiency.[47] Moreover, the "softness" of the interlamellar region correlates directly with the strength of the cohesion energy between adjacent silicate lamellae, which derives mainly from a strong Coulombic interaction that diminishes with distance, and hence basal spacing. For example, Heinz *et al.* used MD simulations to calculate 3.3 and 8.5 times higher cleavage energies for unhydrated K-MMT (layer charge 0.33 *p.f.u.*) and K-mica (layer charge 1.0 *p.f.u.*), respectively, as compared to their corresponding octadecylammonium intercalated forms.[48] Upon intercalation of bulky organocations, the basal spacing increases from 9.98 to 35.16 Å and from 10.18 to 18.8 Å for mica and MMT, respectively.
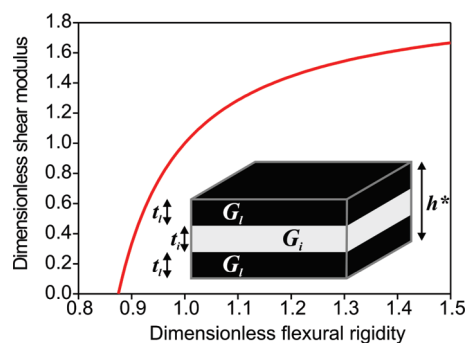
Figure 7. The red curve shows a qualitative estimation of the nonlinear correlation between the shear modulus and flexural rigidity of a sandwich consisting of soft (G_i) and strong (G_l) layers. Details are given in the Supporting Information.

A simple estimation of the shear modulus G_p and the flexural rigidity D_p of thin clay platelets reveals that the stiffness in shear and in bending of a stack of lamellae are related (Figure 7; see Supporting Information for the details of the calculation). G_p hereby consists of two components, the shear moduli of the silicate lamellae (G_l) and the interlayer (G_i). Increasing flexural rigidity is associated with an increasing shear modulus in a highly nonlinear relationship. Consequently, to achieve maximum reinforcement, the mechanical properties of the filler need to be tailored to the specific application and matrix, and there will generally be an optimum height for nanoplatelets.

Strengthening the adhesion, for instance by minimizing the thickness of the interlayer space, will improve the shear strength of clay stacks, thus yielding the desired large flexural strength. On one hand, such a large bending stiffness is of crucial importance for artificial nacre. On the other hand, maximizing the flexural rigidity can also optimize the shear strength in order to prepare PLSNs with high tensile strength. The novel process for the facile production of shear-stiff nanoplatelets is summarized in Scheme 1. To our knowledge, there has only been one report in the literature where mica was successfully exfoliated in a PLSN,[49] but this process is tedious and lengthy. The mica needed to be converted into its organophilized form by prolonged (4 days at 90 °C) heating with a 10-fold excess of the alkylammonium cations. Moreover, exfoliation could only be achieved *in situ* during curing of a particular matrix (epoxy resin) at 180 °C for 6 h. Contrary to this, in the process described here (Scheme 1), exfoliation is achieved in aqueous suspension, and thus crucial properties of the filler like shear-stiffness and aspect ratio are determined prior to compounding and can be ad-

justed independently. Furthermore, the process allows tailoring of both the platelet height and the shear strength. By choosing the appropriate layer charge of 0.5 *p.f.u.*, the interlamellar reactivity of the pristine Na-Hec is very high. The individual steps (cation exchanges, exfoliation) are therefore fast and can be easily incorporated in a technical process to produce shear-stiff, mica-type fillers.

In addition to shear-stiffness, the K-Hec offers a significant economic advantage. The pristine layered silicates are hydrophilic, and it is necessary to adjust the surface tensions of filler and matrix. As already mentioned, the cation exchange for K-Hec is restricted to the outer surfaces (Scheme 1), drastically reducing the amount of compatibilizer required. Commercial organoclays where all external and interlamellar exchange sites are occupied by organocations contain up to 40%/wt of organic matter. With K-Hec, a great deal of these expensive organocations can be "substituted" by cheap K^+ by selective modification of external surfaces. Moreover, alkylammonium cations are known to thermally degrade *via* Hofmann elimination. It is well-known that the concomitant release of volatiles is detrimental to the flame retardant efficiency as the onset temperature is reduced.[50]

CONCLUSIONS

This work describes a fast and facile method to produce shear-stiff, clay-based nanoplatelets with high aspect ratios. Choosing the appropriate layer charge allows for instant switching between shear-labile and shear-stiff states of the same fluorohectorite by simple cation exchange. The two-step process includes physical exfoliation by shearing of a highly swollen, shear-labile form, whereby the degree of exfoliation may be easily tuned and controlled by the shear forces applied. Subsequently, cation exchange with cations with a low enthalpy of hydration induces a collapse of the interlamellar water and produces nonhydrated, mica-like nanoplatelets. The process allows for the independent adjustment of both the platelet height and the shear strength. When combining these ceramic nanoplatelets with polymeric matrices, the mechanical properties of the filler can thus be tailored to the specific application and matrix to achieve maximum reinforcement. Additionally, the mica-like nanoplatelets no longer show interlamellar reactivity. This allows for selective modification of external basal planes only, therefore drastically reducing the amount of compatibilizer needed to produce uniform hybrid materials.

METHODS

Materials. Na-Hec ($\{Na_{0.5}\}^{inter}[Mg_{2.5}Li_{0.5}]^{oct}\langle Si_4 \rangle^{tet}O_{10}F_2$) was synthesized from the melt according to a procedure reported in detail by Breu *et al.*[31]

Standard procedures[51] were applied for cation exchange. One molar aqueous solutions of the chloride salts were used at neutral pH. $GdCl_3$, $ZnCl_2$, $CaCl_2$, $SrCl_2$, $BaCl_2$, RbCl, and CsCl were purchased at p.a. quality from Merck KGaA. $MgCl_2$, LiCl, and KCl were purchased at p.a. quality from Grüssing GmbH. After ion ex-

change, hectorites were dialyzed with a 25–30 Å pore size until the washing water reacted neutrally on a test with $AgNO_3$ for chloride.

A microfluidizer (Microfluidics Inc. type M-110Y) equipped with an H30Z (200 μm, ceramics) and an H10Z (100 μm, diamond) interaction chamber was applied for exfoliation (denoted in the text by shearing cycles) of aqueous suspensions (typically 1 wt %) of fluorohectorites. The operation pressure ranged from 1.0 to 1.2 kbar.

Cation Exchange Capacity (CEC) Measurements. CECs were determined by means of a photometric method (Varian Cary 3 UV–Vis) applying $[Cu(trien)]^{2+}$ as a dye. $CuSO_4$ 99.99+% and triethylene tetramine >97% (trien) were purchased from Sigma Aldrich. The preparation of the complex and the CEC measurements were performed according to procedures in refs 52 and 53. Samples were filtrated using Whatman Anotop 0.1-μm syringe filters prior to photometric measurements.

Specific Surface Measurements (BET). The BET surface area was determined from nitrogen absorption experiments on a Quantachrome Autosorb 1. Five data points within the range of $0.09 < p/p_0 < 0.3$ were taken to calculate the specific surface using the BET equation. All samples were carefully outgassed at 150 °C under ultra high vacuum overnight prior to measurements.

Powder X-ray Diffraction. PXRD patterns are obtained using nickel filtered Cu–Kα radiation (1.54187 Å) on a Bragg–Brentano-type diffractometer (Panalytical XPERT-PRO) equipped with an X'Celerator Scientific RTMS detector. Textured samples were prepared by slow evaporation of aqueous suspensions of fluorohectorite (typically 1%/wt) on planar glass slides (Menzel Gläser Objektträger). For "moist" samples, the supernatant water was removed by contacting the sedimented samples with filter paper and immediately recording the PXRD traces. The dry samples were equilibrated at room temp and 40–45% relative humidity prior to measurement. Therefore, the RH inside the desiccator was adjusted by saturated K_2CO_3-solution.

Topographic Atomic Force Measurements (AFM). AFM imaging was conducted using an Asylum Research MFP3D AFM operating in intermittent contact mode (silicon cantilever with $k_c = 46$ N m^{-1}). The sample was prepared by spin-coating an aqueous K-Hec suspension onto a freshly cleaved mica support.

Supporting Information Available: Equations and mathematical data used in Figures 4 and 7, examples for alkylammonium intercalated organoclays, hydrosorption isotherms of Mg-Hec and Na-Hec at room temp, particle size data (SLS), and powder X-ray diffraction patterns of Na-Hec. This material is available free of charge *via* the Internet at http://pubs.acs.org.

REFERENCES AND NOTES

1. *Handbook of Clay Science*; Bergaya, F.; Theng, B. K. G.; Lagaly, G., Eds.; Developments in Clay Science; Elsevier: Amsterdam, 2006.
2. Bauer, J.; Behrens, P.; Speckbacher, M.; Langhals, H. Composites of Perylene Chromophores and Layered Double Hydroxides: Direct Synthesis, Characterization, and Photo- and Chemical Stability. *Adv. Funct. Mater.* **2003**, *13*, 241–248.
3. Liu, Z. P.; Ma, R. Z.; Osada, M.; Iyi, N.; Ebina, Y.; Takada, K.; Sasaki, T. Synthesis, Anion Exchange, and Delamination of Co-Al Layered Double Hydroxide: Assembly of the Exfoliated Nanosheet/Polyanion Composite Films and Magneto-optical Studies. *J. Am. Chem. Soc.* **2006**, *128*, 4872–4880.
4. Meyn, M.; Beneke, K.; Lagaly, G. Anion-Exchange Reactions of Hydroxy Double Salts. *Inorg. Chem.* **1993**, *32*, 1209–1215.
5. Pienack, N.; Puls, A.; Näther, C.; Bensch, W. The Layered Thiostannate (dienH$_2$)Cu$_2$Sn$_2$S$_6$: A Photoconductive Inorganic–Organic Hybrid Compound. *Inorg. Chem.* **2008**, *47*, 9606–9611.
6. Jiang, T.; Lough, A.; Ozin, G. A.; Bedard, R. L.; Broach, R. Synthesis and Structure of Microporous Layered Tin(IV) Sulfide Materials. *J. Mater. Chem.* **1998**, *8*, 721–732.
7. Fukuda, K.; Akatsuka, K.; Ebina, Y.; Ma, R.; Takada, K.; Nakai, I.; Sasaki, T. Exfoliated Nanosheet Crystallite of Cesium Tungstate with 2D Pyrochlore Structure: Synthesis, Characterization, and Photochromic Properties. *ACS Nano* **2008**, *2*, 1689–1695.
8. Behrens, M.; Riemenschneider, O.; Bensch, W.; Indris, S.; Wilkening, M.; Heitjans, P. Lithium Intercalation into Monoclinic Cr$_4$TiSe$_8$: Synthesis, Structural Phase Transition, and Properties of Li$_x$Cr$_4$TiSe$_8$ ($x = 0.1$–2.8). *Chem. Mater.* **2006**, *18*, 1569–1576.
9. Osada, M.; Sasaki, T. Exfoliated Oxide Nanosheets: New Solution to Nanoelectronics. *J. Mater. Chem.* **2009**, *19*, 2503–2511.
10. Lohmeier, S. J.; Wiebeke, M.; Behrens, P. Lonothermal Synthesis and Characterization of a Layered Propylene Diammonium Gallium Phosphate, (C$_3$H$_{12}$N$_2$)$_6$[Ga$_{12}$P$_{16}$O$_{64}$] · 4.3H$_2$O. *Z. Anorg. Allg. Chem.* **2008**, *634*, 147–152.
11. Maheshwari, S.; Jordan, E.; Kumar, S.; Bates, F. S.; Penn, R. L.; Shantz, D. F.; Tsapatsis, M. Layer Structure Preservation During Swelling, Pillaring, and Exfoliation of a Zeolite Precursor. *J. Am. Chem. Soc.* **2008**, *130*, 1507–1516.
12. According to Lagaly,[13] delamination denotes the complete separation of a clay tactoid into its individual silicate lamellae. Exfoliation describes the cleavage of a tactoid into thinner tactoids. A tactoid is a primary clay platelet that consists of stacked silicate lamellae.
13. Lagaly, G.; Gardolinsky, J. E. F. C. Grafted Organic Derivatives of Kaolinite: II. Intercalation of Primary *n*-Alkylamines and Delamination. *Clay Miner.* **2005**, 547–556.
14. Lotsch, B. V.; Ozin, G. A. Photonic Clays: A New Family of Functional 1D Photonic Crystals. *ACS Nano* **2008**, *2*, 2065–2074.
15. Pinnavaia, T. J.; Park, I.; LeBaron, P. C.; Triantafyllidis, K. S. Epoxy Clay Fabric Film Composites with Unprecedented Oxygen Barrier Properties. *Chem. Mater.* **2006**, *18*, 4393–4398.
16. Kotov, N. A.; Haraszti, T.; Turi, L.; Zavala, G.; Geer, R. E.; Dekany, I.; Fendler, J. H. Mechanism of and Defect Formation in the Self-Assembly of Polymeric Polycation–Montmorillonite Ultrathin Films. *J. Am. Chem. Soc.* **1997**, *119*, 6821–6832.
17. Podsiadlo, P.; Kaushik, A. K.; Arruda, E. M.; Waas, A. M.; Shim, B. S.; Xu, J. D.; Nandivada, H.; Pumplin, B. G.; Lahann, J.; Ramamoorthy, A.; Kotov, N. A. Ultrastrong and Stiff Layered Polymer Nanocomposites. *Science* **2007**, *318*, 80–83.
18. Podsiadlo, P.; Arruda, E. M.; Kheng, E.; Waas, A. M.; Lee, J.; Critchley, K.; Qin, M.; Chuang, E.; Kaushik, A. K.; Kim, H. S.; *et al*. LBL Assembled Laminates With Hierarchical Organization from Nano- to Microscale: High-Toughness Nanomaterials and Deformation Imaging. *ACS Nano* **2009**, *3*, 1564–1572.
19. Bonderer, L. J.; Studart, A. R.; Gauckler, L. J. Bioinspired Design and Assembly of Platelet Reinforced Polymer Films. *Science* **2008**, *319*, 1069–1073.
20. LeBaron, P. C.; Wang, Z.; Pinnavaia, T. J. Polymer Layered Silicate Nanocomposites: An Overview. *Appl. Clay Sci.* **1999**, *15*, 11–29.
21. Schmidt, D.; Shah, D.; Giannelis, E. P. New Advances in Polymer/Layered Silicate Nanocomposites. *Curr. Opin. Solid State Mater. Sci.* **2002**, *6*, 205–212.
22. Tetsuka, H.; Ebina, T.; Nanjo, H.; Mizukami, F. Highly Transparent Flexible Clay Films Modified with Organic Polymer: Structural Characterization and Intercalation Properties. *J. Mater. Chem.* **2007**, *17*, 3545–3550.
23. Paul, D. R.; Robeson, L. M. Polymer Nanotechnology: Nanocomposites. *Polymer* **2008**, *49*, 3187–3204.
24. Manias, E. Nanocomposites - Stiffer by Design. *Nat. Mater.* **2007**, *6*, 9–11.

25. Sheng, N.; Boyce, M. C.; Parks, D. M.; Rutledge, G. C.; Abes, J. I.; Cohen, R. E. Multiscale Micromechanical Modeling of Polymer Clay Nanocomposites and the Effective Clay Particle. *Polymer* **2004**, *45*, 487–506.

26. Kunz, D.; Max, E.; Weinkamer, R.; Lunkenbein, T.; Fery, A.; Breu, J. Deformation Measurements on Thin Clay Tactoids. *Small* **2009**, *5*, 1816–1820.

27. Smectite denotes the class of swellable layered 2:1 silicates with a layer charge between 0.2 and 0.6. Common representatives are hectorite, saponite, montmorillonite, and beidellite among others.

28. Devineau, K.; Bihannic, I.; Michot, L.; Villieras, F.; Masrouri, F.; Cuisinier, O.; Fragneto, G.; Michau, N. *In Situ* Neutron Diffraction Analysis of the Influence of Geometric Confinement on Crystalline Swelling of Montmorillonite. *Appl. Clay Sci.* **2006**, *31*, 76–84.

29. Marry, V.; Malikova, N.; Cadene, A.; Dubois, E.; Durand-Vidal, S.; Turq, P.; Breu, J.; Longeville, S.; Zanotti, J. M. Water Diffusion in a Synthetic Hectorite by Neutron Scattering—Beyond the Isotropic Translational Model. *J. Phys.: Condens. Mat.* **2008**, *20*, 4205.

30. Malikova, N.; Cadene, A.; Dubois, E.; Marry, V.; Durand-Vidal, S.; Turq, P.; Breu, J.; Longeville, S.; Zanotti, J. M. Water Diffusion in a Synthetic Hectorite Clay Studied by Quasi Elastic Neutron Scattering. *J. Phys. Chem. C.* **2007**, *111*, 17603–17611.

31. Breu, J.; Seidl, W.; Stoll, A. J.; Lange, K. G.; Probst, T. U. Charge Homogeneity in Synthetic Fluorohectorite. *Chem. Mater.* **2001**, *13*, 4213–4220.

32. Mariychuk, R.; Baumgartner, A.; Wagner, F. E.; Lerf, A.; Dubbe, A.; Moos, R.; Breu, J. Synthesis, Structure, and Electric Conductivity of Ferrous Tainiolite and its Oxidative Conversion into Coarse-Grained Swellable Smectite. *Chem. Mater.* **2007**, *19*, 5377–5387.

33. Breu, J.; Seidl, W.; Senker, J. Synthese von dreidimensional geordneten Einlagerungsverbindungen des Hectorits (Synthesis of Three-Dimensionally Ordered Intercalation Compounds of Hectorite). *Z. Anorg. Allg. Chem.* **2004**, 80–90.

34. Laird, D. A. Influence of Layer Charge on Swelling of Smectites. *Appl. Clay Sci.* **2006**, *34*, 74–87.

35. Teppen, B. J.; Miller, D. M. Hydration Energy Determines Isovalent Cation Exchange Selectivity by Clay Minerals. *Soil Sci. Soc. Am. J.* **2006**, *70*, 31–40.

36. Maes, A.; Cremers, A. Highly Selective Ion-Exchange in Clay-Minerals and Zeolites. *ACS Symp. Ser.* **1986**, *323*, 254–295.

37. Lagaly G. Hydrationszustand der 2:1-Tonminerale. *Tonminerale und Tone*; Jasmund, K., Lagaly, G., Eds.; Steinkopff Verlag: Darmstadt, Germany, 1993; pp 105−107.

38. Scherrer, P. Bestimmung der Grösse und der inneren Struktur von Kolloidteilchen mittels Röntgenstrahlen (Determining the Size and the Internal Structure of Colloidal Particles by Means of X-rays). *Nachr. Ges. Wiss. Goettingen* **1918**, *2*, 96–100.

39. Thompson, D. W.; Butterworth, J. T. The Nature of Laponite and its Aqueous Dispersions. *J. Colloid Interface Sci.* **1992**, *151*, 236–243.

40. Bowen, P. Particle Size Distribution Measurement from Millimeters to Nanometers and from Rods to Platelets. *J. Dispersion Sci. Technol.* **2002**, *23*, 631–662.

41. Halpin, J. C.; Kardos, J. L. The Halpin-Tsai Equations: A Review. *Polym. Eng. Sci.* **1976**, *16*, 344–352.

42. Hedicke-Höchstötter, K.; Demchuk, V.; Langenfelder, D.; Altstädt, V. Fatigue Crack Propagation Behaviour of Polyamide-6 Nanocomposites Based on Layered Silicates. *J. Plast. Technol.* **2007**, *3*, 1–22.

43. Kunowski, H.; Hofmann, U. Vergleichende Untersuchung von Kautschukfüllstoffen. *Angew. Chem.* **1955**, *67*, 289–300.

44. Kojima, Y.; Usuki, A.; Kawasumi, M.; Okada, A.; Kurauchi, T.; Kamigaito, O. Synthesis of Nylon-6-Clay Hybrid by Montmorillonite Intercalated with ε-Caprolactam. *J. Polym. Sci., Part A* **1993**, *31*, 983–986.

45. Hedicke, K.; Wittich, H.; Mehler, C.; Gruber, F.; Altstädt, V. Crystallisation Behaviour of Polyamide-6 and Polyamide-66 Nanocomposites. *Compos. Sci. Technol.* **2006**, *66*, 571–575.

46. Jordan, J. W. Organophilic Bentonites. I. Swelling in Organic Liquids. *J. Phys. Chem.* **1949**, *53*, 294–306.

47. Brune, D. A.; Bicerano, J. Micromechanics of Nanocomposites: Comparison of Tensile and Compressive Elastic Moduli and Prediction of Effects of Incomplete Exfoliation and Imperfect Alignment on Modulus. *Polymer* **2002**, *43*, 369–387.

48. Heinz, H.; Vaia, R. A.; Farmer, B. L. Interaction Energy and Surface Reconstruction between Sheets of Layered Silicates. *J. Chem. Phys.* **2006**, 124.

49. Tamura, K.; Yokoyama, S.; Pascua, C. S.; Yamada, H. New Age of Polymer Nanocomposites Containing Dispersed High-Aspect-Ratio Silicate Nanolayers. *Chem. Mater.* **2008**, *20*, 2242–2246.

50. Morgan, A. B. Flame Retarded Polymer Layered Silicate Nanocomposites: A Review of Commercial and open Literature Systems. *Polym. Adv. Technol.* **2006**, *17*, 206–217.

51. Carrado, K. A.; Decarreau, A.; Petit, S.; Bergaya, F.; Lagaly, G. Synthetic Clay Minerals and Purification of Natural Clays. *Handbook of Clay Science*; Bergaya, F., Theng, B. K. G., Lagaly, G., Eds.; Elsevier Ltd.: Amsterdam, 2006; pp 115−139.

52. Meier, L. P.; Kahr, G. Determination of the Cation Exchange Capacity (CEC) of Clay Minerals Using the Complexes of Copper(II) Ion with Triethylenetetramine and Tetraethylenepentamine. *Clays Clay Miner.* **1999**, *47*, 386–388.

53. Lagaly, G.; Bergaya, F.; Ammann, L. Determination of the Cation Exchange Capacity of Clays with Copper Complexes Revisited. *Clay Miner.* **2005**, *40*, 441–453.